JNTM JOURNAL of NEW TECHNOLOGY and MATERIALS

Journal of New Technology and Materials

Vol. 16, No. 1 (2025), 8–20

RESEARCH ARTICLE

Reliability-Resolved Ranking of Molecular Additives for Defect-Passivated Mixed-Cation Perovskite Solar Cells

Anthony Leggett[1,*] and W. Lee[2]

[1]Department of Physics, University of Illinois Urbana-Champaign, 1110 West Green Street, Urbana, Illinois 61801-3003, USA. [2]Shanghai Center for Complex Physics, Shanghai Jiaotong University, Shanghai, People's Republic of China

*Correspondence: aleggett@illinois.edu

Received date: December 20, 2025; Accepted date: March 12, 2026

Abstract

While molecular additives are commonly used for the tuning of crystal growth and defect passivation in halide perovskite solar cells, additive selection is often done based on peak efficiency or chemical intuition. In this paper, we seek to determine whether it is possible to rank additive performance in inverted $Cs_{0.05}MA_{0.10}FA_{0.85}PbI_3$ devices using the combination of mechanistic analysis, population statistics, champion-cell retention, and trap density suppression via space charge limited current as an objective index. Four molecular additives are analyzed against the raw reference: 3,5-difluoropyridine-2-carboxylic acid (DFCA), 5-hydroxy-2-methylbenzoic acid (HMBA), gallic acid (GA), and caffeic acid (CA). First, a reasoning gate is applied in order to separate the meaningful additive recommendations from superficial pattern-matching. The photovoltaic reliability is calculated via mean *PCE*, coefficient of variation (CV_{PCE}), and champion-cell performance. A trap density correction is subsequently applied based on the difference in defect density between the reference and additive-modified devices. Among those additives studied, HMBA yields the strongest total score. It leads to the highest mean *PCE* ($18.20 \pm 0.27\%$) and champion *PCE* (18.63%), smallest coefficient of variation (1.48%), and lowest trap density ($1.35 \times 10^{15} \rightarrow 1.03 \times 10^{15}$ cm^{-3}). The other additives show varied performance, although DFCA also leads to an improvement in defect density. Both GA and CA reduce *PCE* and increase the coefficient of variation while failing the reliability requirement despite their multiplicity of polar functional groups.

Keywords: mixed-cation perovskites, additive engineering, defect passivation, trap density, inverted solar cells, reproducibility, reliability index

1 Introduction

Hybrid organic–inorganic halide perovskites have progressed from visible-light sensitizers into the most widely researched absorber class in thin-film photovoltaics. Their rise was facilitated by high absorption efficiencies, long electron and hole diffusion lengths, solution processability, and composition tunability without full reconfiguration of the device structure [1–3]. Initial proof-of-concept studies of solid-state and sequential deposition schemes demonstrated the potential of the perovskite film as an active material rather than a sensitizing dye. Subsequent work has also highlighted that efficient charge extraction is achievable in polycrystalline perovskites. Halide perovskites are hence relevant to technological and material innovation, where chemical synthesis, nanoscale structure, defect chemistry, and device design are inseparable [4, 5].

Formamidinium-rich perovskites exhibit particularly sensitive behavior toward compositional and process optimization. While pure $FAPbI_3$ has an appropriate band gap, it is prone to phase instabilities during fabrication and device operation. Mixed cations (methylammonium) and cesium ions provide stability of the black perovskite phase, moderate crystallization kinetics, and better film uniformity [6, 7]. The chosen composition ($Cs_{0.05}MA_{0.10}FA_{0.85}PbI_3$) reflects the need for a practically applicable absorber whose small compositional changes will impact nucleation, grain growth, electrical disorder, and charge extraction.

The principal challenge for halide perovskite absorbers is not just obtaining an efficient cell, but obtaining a narrow and reliable cell distribution. Grain-boundaries and interfaces of polycrystalline perovskite films host various kinds of point defects. They include shallow donor and acceptor centers, but iodine-related defects and under-coordinated Pb can produce deep traps leading to V_{OC} depression, decreased fill factor, and increased hysteretic responses [8–10]. Since halide perovskites are soft ionic semiconductors, defects can couple to the ion migration process and local band bending [11–13]. This makes the performance distribution dependent on the details of precursor composition, drying, and contact deposition. An effective additive is thus required to reduce both average loss and scatter of the cell distribution.

Additive engineering is a straightforward approach to manipulating chemical and electronic properties of films. Functional groups of an additive can coordinate with under-coordinated Pb, participate in acid-base reactions or hydrogen bonding, and adjust steric accessibility of different sites in the film via aromatic moieties. Depending on the interaction strengths, an additive can extend lifetime of the precursors in solution, create nuclei for crystallization, control grain growth, and suppress disorder after annealing. All these effects can explain why a small molecule may increase all key parameters of the perovskite solar cells simultaneously [14–16]. Interaction of an additive with the surface and grain-boundary defects also plays a critical role in reducing recombination processes [17, 18].

An additive chemistry is not driven by a simple monotonic principle, however. Excessively polar compounds may strongly bond with the active film, interfere with solubility and crystallization of the perovskite, and leave inert material at grain boundaries. Compounds with relatively few functional groups will generate an optimal absorber if their interaction is sufficient to eliminate defects, but insufficient to prevent crystallization and charge transport. This is particularly true for aromatic carboxylic acids and hydroxylated aromatics, as acidity, hydrogen bonding, and aromatic rings combine. The chosen additive set—DFCA, HMBA, GA, and CA—thus serves as an effective way to assess whether a compound interacts with a perovskite precursor within the desirable range.

Comparing champion cells is a common way of reporting results in the field, but it is not adequate for addressing this question. Even though a highest-efficiency cell is an indicator of a processing condition's success, it does not indicate if the process is stable. On the other hand, even a small gain in average performance can be meaningful if it is achieved with minimal variability in device efficiency. Laboratory-scale perovskite photovoltaics thus require population statistics to distinguish between good and bad results [19]. Materials and device information are therefore provided by cell statistics, not just reported alongside it.

Recommendation systems also add complexity to the problem. Informatics approaches based on machine learning and data-driven modeling can accelerate materials search via connecting known properties and descriptors to literature [20–22]. Proper use of data infrastructure and descriptors is necessary even in automated materials screening workflows [23]. Natural language processing techniques and reasoning-oriented models are also actively applied to scientific tasks, as they allow generating predictions for experiments from literature descriptions [24, 25]. Efficient parameter tuning and reasoning prompt methods, in turn, make domain-specific material screening even more relevant, although its recommendations still must be compared with experiment [26, 27]. A recommendation system, however, is useful only if its output is connected to actual measurements. In perovskite photovoltaics, the credibility of a recommendation method is defined not only by plausibility, but also by improving cell efficiency and trap density reduction.

The main research question formulated in this paper is therefore specific and clear: Can a reliability index gated by mechanisms of interaction detect the additive with maximum beneficial impact on mean efficiency, reproducibility, champion-device retention, and trap-density suppression? Instead of maximizing a single property of the perovskite solar cells, this objective aims at finding the additive whose processing scheme produces more stable devices with reduced defects. The answer to this question is given by a reliability index that relies on experimentally measurable quantities.

Three contributions make this study unique. First, additive selection is posed as a reliability-ranking problem, not a peak-efficiency comparison. Second, numerical ranking is related to molecular interaction balance, illustrating why HMBA and DFCA are favorable and GA and CA disruptive additives. Third, reproducible calculation protocol is outlined that can be applied to an expanded additive library once descriptors like binding energy, dipole moments, acidity, steric volume, and solubility become accessible.

2 Device Architecture and Additive-Selection Framework

The analysis considers five device groups prepared in an inverted mixed-cation perovskite architecture: an untreated reference and four precursor-additive treatments. The absorber composition is $Cs_{0.05}MA_{0.10}FA_{0.85}PbI_3$. The additive set contains DFCA, HMBA, GA, and CA. These molecules represent different combinations of carboxylic acid functionality, aromatic structure, heteroatom placement, fluorination, hydroxyl substitution, and conjugation. This diversity is important because it permits a comparison between balanced interaction strength and excessive multifunctionality.

Figure 1 defines the chemical context of the study. The schematic does not treat the additive as a generic passivating agent. Instead, it shows that each molecule must be judged by how it interacts with under-coordinated lead centers, grain-boundary disorder, and local crystallization pathways in the perovskite layer. The purpose of the reliability index is to decide which molecule produces the most favorable device-level consequence of these microscopic interactions.

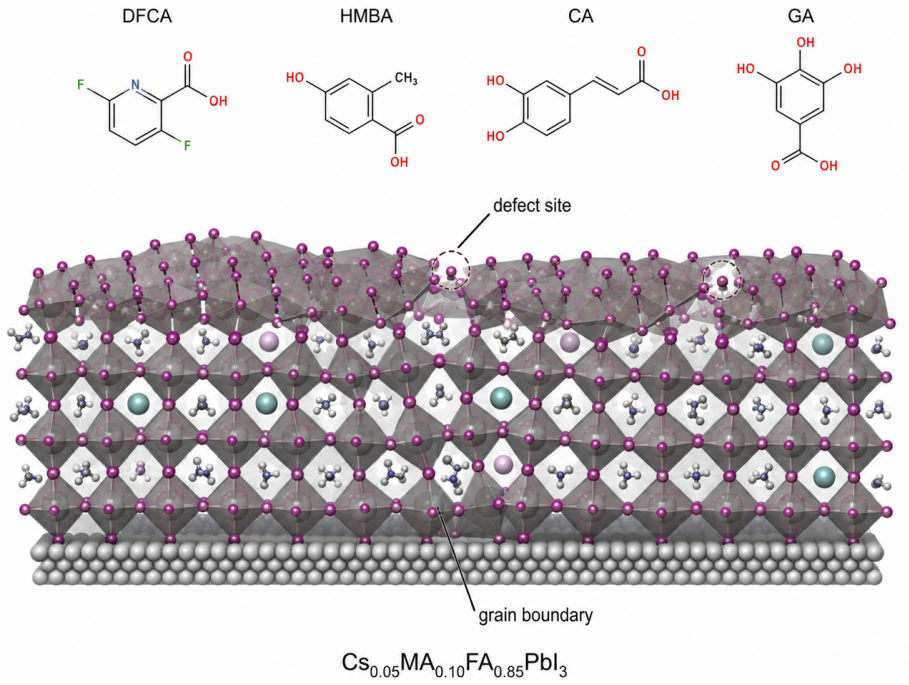

Figure 1. Chemical setting for the reliability study. The four additives are positioned relative to a mixed-cation perovskite absorber to emphasize that passivation, crystallization moderation, and grain-boundary interaction occur together rather than as independent events. The figure motivates why additive evaluation must include photovoltaic statistics and trap-density evidence.

A preliminary reasoning gate was used because additive selection requires coordinated chemical and device-level interpretation. For model m, the weighted reasoning reliability value was defined as

$$R_m = 0.20A_{\text{easy}} + 0.30A_{\text{medium}} + 0.50A_{\text{hard}}, \tag{1}$$

where A_{easy}, A_{medium}, and A_{hard} are the accuracies obtained for three classes of perovskite-related questions.

Eq. 1 is deliberately asymmetric. The hard-question term has the largest weight because the practical additive decision is closer to a difficult mechanistic reasoning problem than to a factual recall problem. A molecule must be assessed in terms of coordination chemistry, film formation, defect passivation, electronic loss, and reproducibility at the same time. A model that performs well on easy questions but poorly on difficult ones should not dominate the additive recommendation.

3 Photovoltaic Population Reliability Metrics

For each additive condition i, the mean-efficiency response relative to the untreated reference was calculated as

$$\eta_i = \frac{\overline{\text{PCE}}_i}{\overline{\text{PCE}}_0}, \tag{2}$$

where $\overline{\text{PCE}}_0$ denotes the mean efficiency of the untreated reference group. This ratio isolates the average gain or loss caused by the additive. A value above unity means that the device population improved in mean efficiency; a value below unity means that the additive reduced the average photovoltaic output.

The width of the device population was represented by the coefficient of variation,

$$CV_i = \frac{\sigma_{\text{PCE},i}}{\overline{\text{PCE}}_i}. \tag{3}$$

Eq. 3 is important because the standard deviation alone is difficult to compare when the mean efficiency changes strongly among treatments. Normalizing the spread by the mean PCE makes the value a relative reproducibility indicator. A lower CV_i indicates a tighter fabrication response and a lower probability of producing weak cells.

The reproducibility factor was then assigned as

$$\rho_i = \frac{1}{1 + CV_i}. \tag{4}$$

This transformation converts the coefficient of variation into a multiplicative penalty. Broad distributions receive a smaller ρ_i, while tightly grouped devices remain close to unity. The form is intentionally simple and monotonic so that the statistical meaning of the correction remains clear.

Champion-cell retention was calculated using

$$\chi_i = \frac{\mathrm{PCE}_i^{\mathrm{champ}}}{\mathrm{PCE}_0^{\mathrm{champ}}}. \tag{5}$$

The champion term prevents the index from rewarding a treatment that narrows the distribution only by suppressing all devices to a lower performance level. A useful additive should maintain or improve the best cell while also raising the average and reducing scatter.

The photovoltaic reliability term was obtained from

$$\Phi_i = \eta_i \rho_i \chi_i. \tag{6}$$

Eq. 6 requires simultaneous success in three directions: the mean device must improve, the device set must become more uniform, and the best device must not be sacrificed. This product form is stricter than a weighted sum because a serious failure in one term directly suppresses the final photovoltaic reliability value.

4 Trap-Density Correction and Final Reliability Index

Trap-density information was incorporated because a photovoltaic improvement is more convincing when it is accompanied by a reduction in electronically active defects. In space-charge-limited-current analysis, the trap density is commonly related to the trap-filled-limit voltage through

$$N_t = \frac{2\varepsilon_r \varepsilon_0 V_{\mathrm{TFL}}}{eL^2}, \tag{7}$$

where ε_r is the relative dielectric constant, ε_0 is the vacuum permittivity, V_{TFL} is the trap-filled-limit voltage, e is the elementary charge, and L is the active-layer thickness.

Eq. 7 clarifies the physical meaning of the trap-density comparison. When thickness and dielectric assumptions are held constant, a lower V_{TFL} corresponds to a lower estimated trap density. The value should still be interpreted as a comparative device-quality indicator rather than as an isolated microscopic count, because SCLC analysis can be affected by contact selectivity, mobile ions, and field distribution [28, 29]. Within a consistent set of samples, however, the relative trend is useful for judging whether the additive suppresses trap-mediated recombination.

The relative trap-density suppression was defined as

$$\Delta N_{t,i} = 1 - \frac{N_{t,i}}{N_{t,0}}, \tag{8}$$

where $N_{t,0}$ is the trap density of the untreated reference. Positive values of $\Delta N_{t,i}$ indicate that the additive lowers the trap density, while a zero value corresponds to no improvement relative to the reference.

The final defect-corrected reliability index was calculated as

$$\Psi_i = \Phi_i(1 + \Delta N_{t,i}). \tag{9}$$

This final term rewards additives that combine photovoltaic improvement with electronic-defect suppression. It also separates a true passivating additive from a molecule that gives a small efficiency increase without reducing the defect population. The index therefore remains interpretable: Φ_i describes device-population reliability, while Ψ_i adds the defect-quality gate.

5 Mechanistic Reasoning and Photovoltaic Response Screening

Table 1 summarizes the three-level reasoning accuracy and the weighted value obtained from Eq. 1. The domain-specialized model has the highest reliability score, $R_m = 82.64$, while GLM-4.5-Air follows with $R_m = 74.34$. The key separation occurs in the hard-question category, where the leading model reaches 78.79%. This matters because the molecular-additive problem requires simultaneous interpretation of binding, acid–base chemistry, crystallization, trap passivation, and full-device response.

Table 1. Reasoning performance used to screen the chemical recommendation step before photovoltaic ranking.

Model	Easy (%)	Medium (%)	Hard (%)	R_m
DeepSeek-R1	47.95	41.76	39.39	41.81
Gemini-2.5-Pro	71.23	60.44	42.42	53.59
QwQ-32B	73.97	61.54	48.48	57.50
Phi-4-Reasoning	76.71	69.23	66.67	69.45
GLM-4.5-Air	79.45	73.63	72.73	74.34
Llama-3.3-70B-Instruct	82.19	81.32	54.55	68.11
Perovskite-R1	87.67	85.71	78.79	82.64

Table 1 is not used to claim that reasoning accuracy alone proves additive success. Rather, it defines a confidence filter. A model can only guide molecular selection if it performs well on the most difficult class of perovskite questions. The table therefore places chemical recommendation before, but not above, device-level evidence.

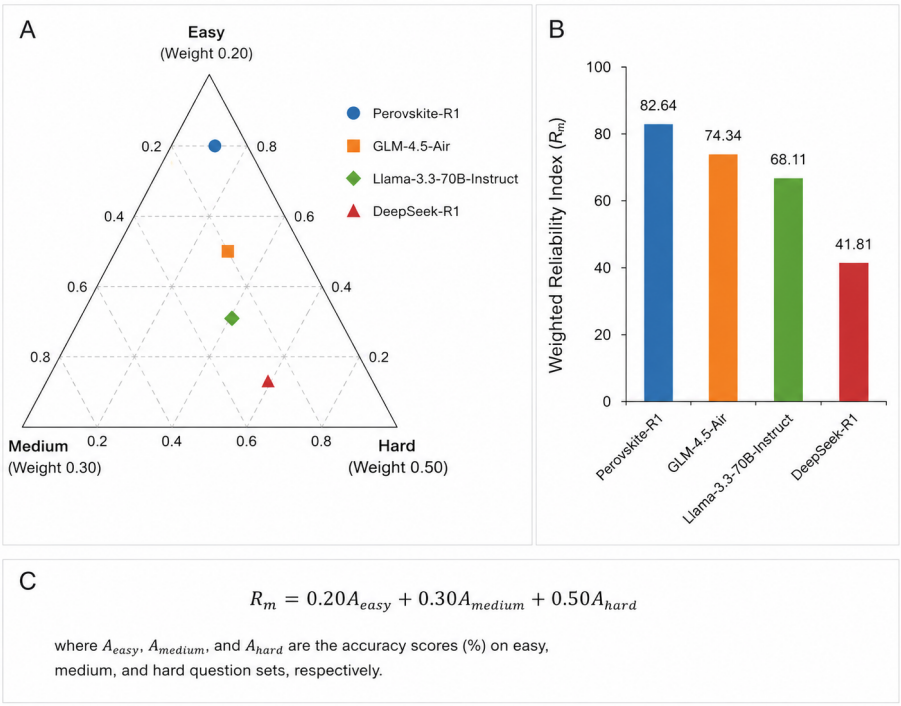

Figure 2. Weighted reasoning gate for additive recommendation. The figure compares easy, medium, and hard perovskite-question performance and shows how the final R_m value gives greatest influence to the hard category, where chemically coupled interpretation is required.

Figure 2 shows why the hard-question weight is necessary. The domain-specialized model separates most clearly from the other models when the question requires mechanistic integration, not simple recognition. This supports the decision to use the model output only as the first gate and to let the experimental statistics decide the final additive ranking.

The mean photovoltaic parameters are listed in Table 2. The untreated reference has $V_{OC} = 1.071 \pm 0.014$ V, $J_{SC} = 21.39 \pm 0.43$ mA cm^{-2}, $FF = 73.70 \pm 1.95\%$, and $PCE = 17.38 \pm 0.72\%$. DFCA and HMBA improve the average response, reaching $18.12 \pm 0.28\%$ and $18.20 \pm 0.27\%$, respectively. Their gains are not caused by a single parameter. Both maintain high voltage, increase current density, preserve fill factor, and substantially reduce the spread of the device group.

Table 2. Mean photovoltaic parameters of untreated and additive-treated inverted mixed-cation perovskite solar cells.

Sample	V_{OC} (V)	J_{SC} (mA cm^{-2})	FF (%)	PCE (%)
Control	1.071 ± 0.014	21.39 ± 0.43	73.70 ± 1.95	17.38 ± 0.72
GA	0.951 ± 0.024	19.82 ± 0.67	56.50 ± 3.76	8.76 ± 1.20
CA	0.972 ± 0.023	20.09 ± 0.48	66.18 ± 3.09	12.46 ± 0.83
DFCA	1.087 ± 0.011	22.19 ± 0.17	75.00 ± 1.28	18.12 ± 0.28
HMBA	1.086 ± 0.006	22.41 ± 0.14	74.89 ± 1.27	18.20 ± 0.27

Table 2 reveals two distinct additive classes. HMBA and DFCA shift the average device response upward while making

the uncertainty interval narrower. GA and CA move the response downward and broaden it. The strong reduction in *FF* for GA, from 73.70% in the reference to 56.50%, is especially important because it points to charge-extraction or recombination losses rather than a purely optical limitation.

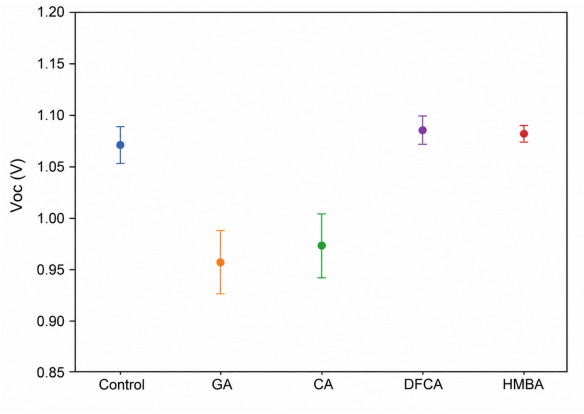

Figure 3. Open-circuit-voltage comparison for the five device groups. HMBA and DFCA retain the voltage level of the reference devices, whereas GA and CA show voltage loss consistent with increased non-radiative recombination or less favorable interfacial energetics.

Figure 3 indicates that the beneficial additives do not improve current by sacrificing voltage. DFCA gives the highest mean V_{OC}, and HMBA remains statistically close to it. In contrast, GA and CA lose approximately 0.12 and 0.10 V relative to the untreated reference, showing that their chemistry introduces or fails to suppress recombination-active pathways.

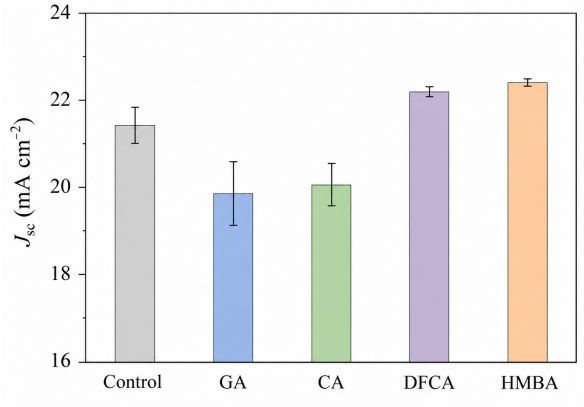

Figure 4. Short-circuit-current-density response after additive treatment. The higher J_{SC} values of HMBA and DFCA indicate improved charge generation or collection, while GA and CA remain below the untreated reference.

Figure 4 gives the clearest evidence that HMBA and DFCA improve the absorber/contact combination rather than merely altering the voltage. HMBA increases J_{SC} to 22.41 ± 0.14 mA cm^{-2}, the highest value in the set. The narrow uncertainty also suggests that the current gain is repeatable across the measured population.

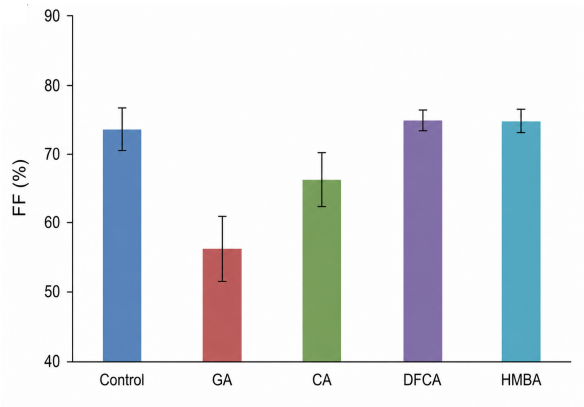

Figure 5. Fill-factor response of the untreated and additive-treated cells. The strong loss for GA and the moderate loss for CA indicate transport or recombination penalties, whereas HMBA and DFCA preserve the rectangularity of the current–voltage curve.

Figure 5 separates chemically balanced additives from disruptive additives. HMBA and DFCA maintain fill factors near 75%, while GA falls to 56.50%. Because fill factor is sensitive to recombination, series resistance, shunt pathways, and extraction barriers, this result shows that excessive or poorly balanced additive interaction can damage operational device quality even when the molecule contains passivating groups.

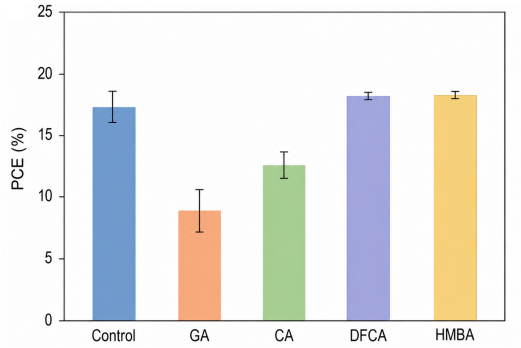

Figure 6. Mean power-conversion efficiency of the five device groups. HMBA and DFCA provide moderate but reproducible gains over the untreated reference, while GA and CA cause large efficiency penalties.

Figure 6 summarizes the average-output consequence of the preceding voltage, current, and fill-factor trends. HMBA gives the highest mean efficiency, and DFCA is nearly equivalent. The small absolute gain should not be dismissed, because it is accompanied by a much lower scatter. The efficiency loss for GA and CA confirms that a molecule can be chemically plausible but practically unsuitable for this perovskite composition.

6 Device-Population Reliability and Defect-Corrected Ranking

Table 3 converts the average *PCE*, distribution width, and champion response into the photovoltaic reliability term Φ_i. HMBA gives the strongest photovoltaic-only value, $\Phi_i = 1.050$, and DFCA follows closely with $\Phi_i = 1.042$. The untreated reference has $\Phi_i = 0.960$ because the reproducibility term is below unity even before additive comparison. GA and CA are sharply penalized because their lower efficiencies are accompanied by broader distributions.

Table 3. Derived efficiency and reproducibility quantities used to calculate the photovoltaic reliability term.

Sample	Mean *PCE* gain (%)	CV_{PCE} (%)	ρ_i	Φ_i
Control	0.00	4.14	0.960	0.960
GA	-49.60	13.70	0.880	0.280
CA	-28.31	6.66	0.938	0.495
DFCA	4.26	1.55	0.985	1.042
HMBA	4.72	1.48	0.985	1.050

The most important information in Table 3 is the simultaneous change in gain and scatter. HMBA raises the mean *PCE* by 4.72% relative to the reference while lowering CV_{PCE} from 4.14% to 1.48%. DFCA gives a 4.26% gain and lowers CV_{PCE} to 1.55%. These are reliability improvements, not only efficiency improvements. They imply that the additives reduce sensitivity to small processing variations and promote more uniform absorber formation.

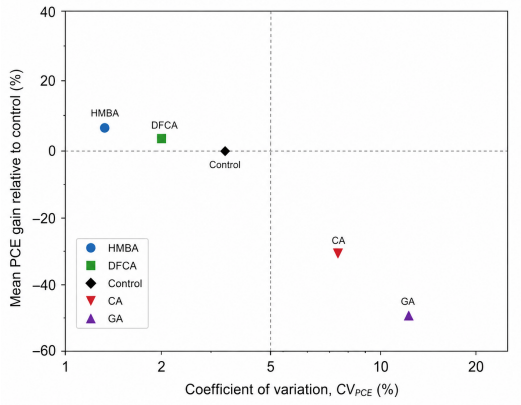

Figure 7. Efficiency-gain and distribution-width map. The reliable region corresponds to positive mean *PCE* gain combined with low CV_{PCE}; HMBA and DFCA occupy this region, whereas GA and CA combine negative gain with larger population scatter.

Figure 7 visualizes why average efficiency alone is insufficient. A candidate should be located above the no-gain line and toward the low-variation side of the map. HMBA and DFCA satisfy both requirements. GA and CA fail both requirements, demonstrating that their molecular functionality does not translate into a reliable device population.

The close photovoltaic-only values of HMBA and DFCA also show why a defect correction is necessary. If only Φ_i is considered, the two additives appear almost equivalent. That conclusion would be incomplete because it does not yet ask whether the electronic trap landscape has been improved. The following trap-density analysis therefore determines whether the slight photovoltaic advantage of HMBA is supported by a stronger physical defect signature.

The champion-cell parameters are given in Table 4. The untreated reference reaches 18.30% champion *PCE*. DFCA improves the champion value to 18.58%, and HMBA gives the highest champion result, 18.63%. The absolute gain is modest, but the difference becomes meaningful when read together with the mean data. A higher champion value with a narrow distribution indicates a broadened processing window rather than a rare outlier.

Table 4. Photovoltaic parameters of the champion devices from each treatment group.

Sample	V_{OC} (V)	J_{SC} (mA cm^{-2})	*FF* (%)	*PCE* (%)
Control	1.097	21.92	76.15	18.30
GA	0.966	20.48	58.40	11.56
CA	0.971	20.45	67.82	13.47
DFCA	1.097	22.17	76.40	18.58
HMBA	1.087	22.27	76.93	18.63

Table 4 confirms that HMBA and DFCA do not obtain reliability by suppressing high-performing devices. Both maintain champion performance above the untreated reference, with HMBA giving the strongest champion *PCE* and the highest champion fill factor. GA and CA remain far below the reference even in their best cells, which means their poor average response cannot be explained only by a few defective outliers.

Figure 8 supports the use of χ_i in Eq. 6. HMBA and DFCA display high champion values without a large gap from their means. This is the desired pattern for additive engineering, because it indicates that the best device is representative of the processing condition. The GA and CA groups show the opposite pattern: even their champions remain inefficient, so their molecular interaction with the precursor environment is unfavorable under the examined conditions.

Trap-density parameters and final reliability values are shown in Table 5. The untreated reference has $N_t = 1.35 \times 10^{15}$ cm^{-3}. DFCA reduces this value to 1.26×10^{15} cm^{-3}, corresponding to 6.67% trap suppression. HMBA produces a much larger reduction, 1.03×10^{15} cm^{-3}, corresponding to 23.70% trap suppression. This difference changes the final interpretation of the two beneficial additives.

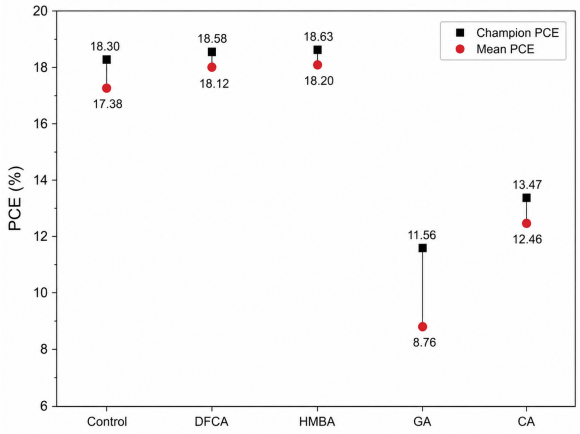

Figure 8. Champion and mean efficiency comparison. HMBA and DFCA show small champion–mean separations, indicating repeatable high performance; GA and CA show low mean values and weak champion retention.

Table 5. Trap-density parameters and final defect-corrected reliability values.

Sample	V_{TFL} (V)	N_t ($\times 10^{15}$ cm^{-3})	ΔN_t (%)	Ψ_i
Control	0.162	1.35	0.00	0.960
DFCA	0.151	1.26	6.67	1.112
HMBA	0.124	1.03	23.70	1.299

Table 5 answers the question that Φ_i could not answer alone. HMBA is not merely marginally better in efficiency statistics; it also gives a much stronger reduction in trap density. The decrease in V_{TFL} from 0.162 V to 0.124 V is consistent with fewer trap states being filled before the trap-filled-limit transition. This supports the interpretation that HMBA improves electronic quality in addition to improving population-level efficiency.

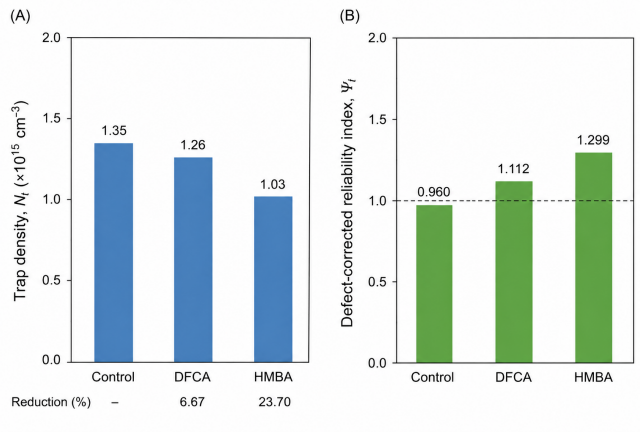

Figure 9. Trap-density response and defect-corrected reliability ranking. The lower trap density of HMBA gives a larger correction to Ψ_i than DFCA, converting a small photovoltaic advantage into a clear defect-quality advantage.

Figure 9 shows the decisive separation between HMBA and DFCA. DFCA improves the device population, but HMBA improves the population and the trap-density signature more strongly. The final ranking is therefore HMBA > DFCA > untreated reference. This order is physically meaningful because it combines efficiency, reproducibility, champion retention, and defect suppression.

7 Molecular Interaction Balance and Materials-Design Implications

Figure 10 places the four additives on a qualitative interaction-balance scale. The key message is that additive success depends on balanced interaction strength. A molecule must bind or hydrogen-bond sufficiently to passivate defect sites, but it must not interfere strongly enough to damage precursor assembly, grain growth, or charge extraction.

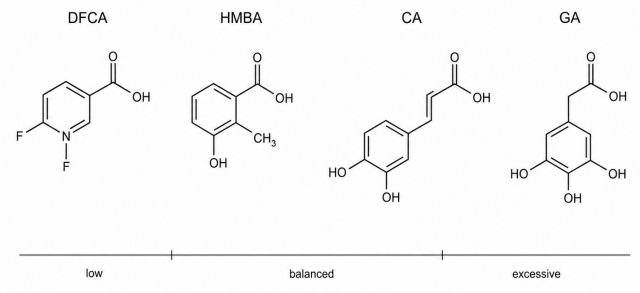

Figure 10. Interaction-balance interpretation of the additive series. HMBA and DFCA fall in the balanced region where passivation and crystallization control can coexist; GA and CA occupy the stronger-interaction side, where excessive multifunctionality may disturb film formation and charge extraction.

The HMBA is clearly the additive with the best performance profile, because it has an appropriate carboxylic acid, hydroxyl substituent, and methyl-substituted aromatic structure. The latter two allow the carboxyl group to interact with lead-rich sites or ionic defects, while providing sufficient modulation of packing/stericity to prevent too dense interactions. The consistency between higher average PCE, reduced CV_{PCE}, good retention, and large trap-density reduction is clear.

The DFCA is quite different, but no less impressive. It has the appropriate polar and electronic functionalities, including a pyridine nitrogen, carboxylic acid group, and fluorinated aromatic ring. The device statistics indicate that the chemistry of the additive does not interfere with the preparation of the perovskite precursor layer. The smaller trap-density reduction in comparison to HMBA indicates that DFCA contributes better to improved uniformity/performance than it does to suppression of electronic traps.

The GA and CA illustrate the potential hazard of taking an additive evaluation based on its functional-group chemistry too literally. They have a number of hydroxyls, along with a carboxylic acid, and a conjugated aromatic acid structure, re-

spectively. Despite the seemingly promising chemistry, the results indicate that the molecule produces either insufficiently weak interactions with the device or causes some other problems. The significant *FF* reduction for GA and large negative mean *PCE* shifts for GA and CA both point to problems with the passivation, which are due to increased recombination and transport barriers.

This method of analysis is effective since the optimal additive can be found based on several meaningful experimentally derived parameters. Figure 11 provides a compact view of efficiency, uniformity, and trapping statistics for the considered additives. This map is particularly useful for materials science because it allows differentiation between molecules that are suitable for device fabrication and those that merely fit well from a purely chemical point of view.

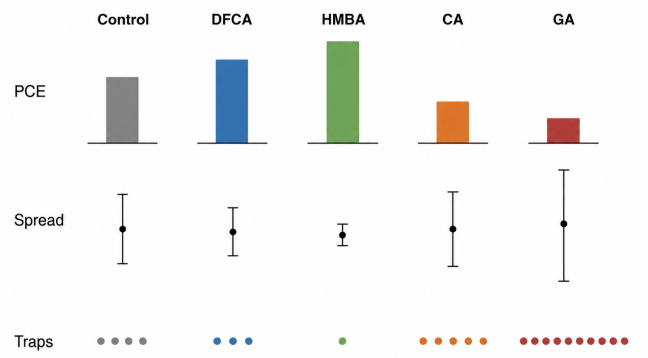

Figure 11. Compact screening map linking average *PCE*, device-population spread, and trap-density evidence. HMBA and DFCA satisfy the reliability requirements, whereas CA and GA are rejected because their efficiency loss and wider scatter dominate any nominal passivation advantage.

Figure 11 also clarifies the role of missing trap-density information for GA and CA. These additives already fail the photovoltaic population criteria, so they do not require a positive defect correction to be rejected. In a larger additive library, however, candidates with moderate photovoltaic response would need the same trap-density gate before being accepted as reliable.

Sample	Mean PCE response	PCE spread (CV_{PCE})	Champion retention (champion – mean)	Trap-density evidence	Mechanistic interpretation
Control	— (0%)	4.14%	0.92%	—	Reference
DFCA	↑ +4.26%	1.55%	0.46%	↓ 6.67% reduction	Beneficial passivation
HMBA	↑ +4.72%	1.48%	0.43%	↓ 23.70% reduction	Balanced passivation
CA	↓ –28.31%	6.66%	1.01%	—	Excessive interaction
GA	↓ –49.60%	13.70%	2.80%	—	Over-functionalization /disruption

Figure 12. Integrated quantitative summary of the additive response. The figure connects efficiency gain, CV_{PCE}, champion retention, trap-density evidence, and chemical interpretation, showing that HMBA is the only additive with the strongest positive response across all available gates.

Figure 12 prevents the conclusion from being reduced to a single score. HMBA leads because all available indicators point in the same direction. DFCA remains a strong secondary candidate because its efficiency and reproducibility response are favorable, even though its defect correction is smaller. GA and CA are excluded because their population statistics are inconsistent with reliable absorber formation.

The material choice is summarized in Figure 13. The material with highest priority should be HMBA since it shows the best performance among all of the materials examined. If reproducibility improvement and lower trap suppression performance is important, then DFCA is the better choice. The reference material is more reliable than the other two choices since GA and CA tend to increase error in their efficiency values. These rankings provide a direct answer to the research question posed at the beginning. Yes, a gate reliability index allows differentiating the best additive more efficiently than using peak efficiencies or functional group differences.

There are multiple applications of this approach that could be beneficial in further additive screening process. Firstly, each additive must be ranked according to its statistical distribution of the output variable. Secondly, one must take the defect density into account since they will help determine whether any increase in performance can be attributed

to any change in electronics quality. Thirdly, molecular descriptors must be chosen to characterize interaction balance: lead binding, acid-base properties, hydrogen-bond forming ability, polarity, steric effects, and compatibility with the solvent-precursor combination. Thus, the approach can be extended to larger libraries.

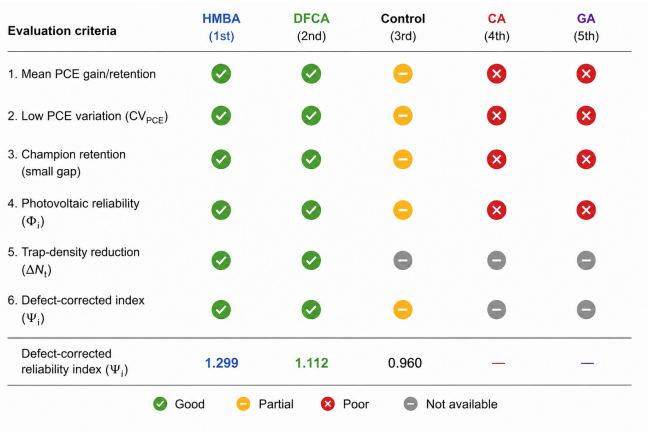

Figure 13. Final decision matrix for the mechanism-gated reliability analysis. The matrix identifies which additives satisfy the mean-efficiency, reproducibility, champion-retention, trap-density, and molecular-balance criteria, giving a final order of HMBA, DFCA, untreated reference, CA, and GA.

The presented analysis also has its limitations. The results were obtained based on compact statistics and not from raw current-voltage data, stabilized power output, intensity dependence, impedance spectroscopy or any aging test data. Also, the trap density data is available for the reference sample, DFCA, and HMBA. As a result, the index is more suitable for ranking the reliability of existing samples than creating a full degradation model. In order to expand the range of possibilities, future analysis will have to include active area estimation, scan direction comparison, and maximum power point tracking.

8 Conclusion

In this study, we considered the question of whether additive selection in inverted $Cs_{0.05}MA_{0.10}FA_{0.85}PbI_3$ perovskite solar cells can benefit from the integration of mechanistic understanding, photovoltaic response at the population level, champion-device selection, and trap density control. Our approach is positive on all counts. We designed an index that distinguishes additives leading to improvement in the entire device population from those whose structure contains potentially useful passivating groups, while also revealing that the optimal molecule is not the one with the most number of functionalities, but one whose intermolecular interaction strength is well-balanced to facilitate improved crystallization without interfering with charge transport. Of the four investigated additives, HMBA is found to be the most reliable option since it maximizes the mean PCE at $18.20 \pm 0.27\%$, yields the highest champion PCE of 18.63%, results in the most narrow $CV_{PCE} = 1.48\%$, and causes the greatest reduction in trap densities from 1.35×10^{15} to 1.03×10^{15} cm^{-3}. Therefore, it gives rise to the maximum defect-corrected reliability index, $\Psi_i = 1.299$. DFCA comes in second place, as it achieves the increased mean PCE value of $18.12 \pm 0.28\%$, CV_{PCE} of 1.55%, and also yields a positive defect correction, though its impact on trap density is less pronounced. At the same time, GA and CA cannot be recommended for this set of devices since they significantly lower the mean PCE: $8.76 \pm 1.20\%$ and $12.46 \pm 0.83\%$, respectively, as well as increase voltage drops and broaden efficiency distributions. These data reveal that even when using molecules containing multiple hydroxyl groups and aromatic acid function, passivation effects can still be overshadowed by their adverse impact on precursor chemistry or charge extraction. This makes the proposed reliability-index approach helpful for materials screening because it maintains transparency of the ranking process, wherein each parameter corresponds to a meaningful experimental characteristic, such as mean efficiency, efficiency dispersion, champion device retention, and defect suppression. For additive discovery in the future, this method should be extended with molecular characterization techniques, stability tests, and descriptors of performance.

References

[1] Kojima, A., Teshima, K., Shirai, Y. & Miyasaka, T. Organometal halide perovskites as visible-light sensitizers for photovoltaic cells. *Journal of the American Chemical Society* 131, 6050–6051 (2009).

[2] Kim, H.-S. et al. Lead iodide perovskite sensitized all-solid-state submicron thin film mesoscopic solar cell with efficiency exceeding 9%. *Scientific Reports* 2, 591 (2012).

[3] Lee, M. M., Teuscher, J., Miyasaka, T., Murakami, T. N. & Snaith, H. J. Efficient hybrid solar cells based on meso-superstructured organometal halide perovskites. *Science* 338, 643–647 (2012).

[4] Hodes, G. Perovskite-based solar cells. *Science* 342, 317–318 (2013).

[5] Green, M. A., Ho-Baillie, A. & Snaith, H. J. The emergence of perovskite solar cells. *Nature Photonics* 8, 506–514 (2014).

[6] Jeon, N. J. et al. Compositional engineering of perovskite materials for high-performance solar cells. *Nature* 517, 476–480 (2015).

[7] Saliba, M. et al. Cesium-containing triple cation perovskite solar cells: improved stability, reproducibility and high efficiency. *Energy & Environmental Science* 9, 1989–1997 (2016).

[8] Yin, W.-J., Shi, T. & Yan, Y. Unusual defect physics in $CH_3NH_3PbI_3$ perovskite solar cell absorber. *Applied Physics Letters* 104, 063903 (2014).

[9] Shao, Y., Xiao, Z., Bi, C., Yuan, Y. & Huang, J. Origin and elimination of photocurrent hysteresis by fullerene passivation in $CH_3NH_3PbI_3$ planar heterojunction solar cells. *Nature Communications* 5, 5784 (2014).

[10] deQuilettes, D. W. et al. Impact of microstructure on local carrier lifetime in perovskite solar cells. *Science* 348, 683–686 (2015).

[11] Tress, W. et al. Understanding the rate-dependent J–V hysteresis, slow time component, and aging in $CH_3NH_3PbI_3$ perovskite solar cells: the role of a compensated electric field. *Energy & Environmental Science* 8, 995–1004 (2015).

[12] Niu, G., Guo, X. & Wang, L. Review of recent progress in chemical stability of perovskite solar cells. *Journal of Materials Chemistry A* 3, 8970–8980 (2015).

[13] Park, N.-G., Gratzel, M., Miyasaka, T., Zhu, K. & Emery, K. Towards stable and commercially available perovskite solar cells. *Nature Energy* 1, 16152 (2016).

[14] Noel, N. K. et al. Lead iodide excess as a route to enhanced performance in perovskite solar cells. *Energy & Environmental Science* 7, 3061–3068 (2014).

[15] Nie, W. et al. High-efficiency solution-processed perovskite solar cells with millimeter-scale grains. *Science* 347, 522–525 (2015).

[16] Yang, W. S. et al. Iodide management in formamidinium-lead-halide-based perovskite layers for efficient solar cells. *Science* 356, 1376–1379 (2017).

[17] Zheng, X. et al. Defect passivation in hybrid perovskite solar cells using quaternary ammonium halide anions and cations. *Nature Energy* 2, 17102 (2017).

[18] Chen, B., Rudd, P. N., Yang, S., Yuan, Y. & Huang, J. Imperfections and their passivation in halide perovskite solar cells. *Chemical Society Reviews* 48, 3842–3867 (2019).

[19] Correa-Baena, J.-P. et al. The rapid evolution of highly efficient perovskite solar cells. *Energy & Environmental Science* 10, 710–727 (2017).

[20] Ramprasad, R., Batra, R., Pilania, G., Mannodi-Kanakkithodi, A. & Kim, C. Machine learning in materials informatics: recent applications and prospects. *npj Computational Materials* 3, 54 (2017).

[21] Butler, K. T., Davies, D. W., Cartwright, H., Isayev, O. & Walsh, A. Machine learning for molecular and materials science. *Nature* 559, 547–555 (2018).

[22] Schmidt, J., Marques, M. R. G., Botti, S. & Marques, M. A. L. Recent advances and applications of machine learning in solid-state materials science. *npj Computational Materials* 5, 83 (2019).

[23] Himanen, L., Geurts, A., Foster, A. S. & Rinke, P. Data-driven materials science: status, challenges, and perspectives. *Advanced Science* 6, 1900808 (2019).

[24] Vaswani, A. et al. Attention is all you need. In *Advances in Neural Information Processing Systems* 30, 5998–6008 (2017).

[25] Brown, T. B. et al. Language models are few-shot learners. In *Advances in Neural Information Processing Systems* 33, 1877–1901 (2020).

[26] Wei, J. et al. Chain-of-thought prompting elicits reasoning in large language models. In *Advances in Neural Information Processing Systems* 35, 24824–24837 (2022).

[27] Hu, E. J. et al. LoRA: low-rank adaptation of large language models. In *International Conference on Learning Representations* (2022).

[28] Lampert, M. A. Simplified theory of space-charge-limited currents in an insulator with traps. *Physical Review* 103, 1648–1656 (1956).

[29] Murgatroyd, P. N. Theory of space-charge-limited current enhanced by Frenkel effect. *Journal of Physics D: Applied Physics* 3, 151–156 (1970).